Biomaterials 314 (2025) 122871

Contents lists available at ScienceDirect

Biomaterials

journal homepage: www.elsevier.com/locate/biomaterials

Enhancing CAR-T cell therapy against solid tumor by drug-free triboelectric immunotherapy

Haimei Li [a,b], Zichen Wang [a,b], Yulin Hu [a,b], Guangqin He [a,b], Liang Huang [f,g], Yi Liu [c,e,**], Zhong Lin Wang [d,***], Peng Jiang [a,b,*]

[a] Department of Orthopedics Trauma and Microsurgery, Zhongnan Hospital of Wuhan University, School of Pharmaceutical Sciences, Wuhan University, Wuhan 430071, China
[b] Key Laboratory of Combinatorial Biosynthesis and Drug Discovery (MOE), Wuhan University, Wuhan 430072, China
[c] School of Chemistry and Materials Sciences & School of Pharmaceutical Sciences, South-Central Minzu University, Wuhan 430074, China
[d] Beijing Institute of Nanoenergy and Nanosystems, Chinese Academy of Sciences, Beijing 100083, China
[e] Hubei Key Laboratory of Radiation Chemistry and Functional Materials, School of Nuclear Technology and Chemistry and Biology, Hubei University of Science and Technology, Xianning 437100, China
[f] State Key Laboratory of Experimental Hematology, National Clinical Research Center for Blood Diseases, Haihe Laboratory of Cell Ecosystem, Institute of Hematology & Blood Diseases Hospital, Chinese Academy of Medical Science & Peking Union Medical College, Tianjin 300020, China
[g] Tianjin Institutes of Health Science, Tianjin 301600, China

ARTICLE INFO

Keywords:
CAR-T cell
Solid tumor treatment
Triboelectric immunotherapy
Immunosuppressive microenvironment
Triboelectric nanogenerator

ABSTRACT

Chimeric antigen receptor (CAR) T cell therapy is a highly effective immunotherapy for hematological tumors, but its efficacy against most solid tumors remains challenging. Herein, a novel synergistic combination therapy of drug-free triboelectric immunotherapy and CAR-T cell therapy against solid tumor was proposed. A triboelectric nanogenerator (TENG) that can generate pulsed direct-current by coupling triboelectrification effect and electrostatic breakdown effect was fabricated. The TENG can generate up to 30 pulse direct-current peaks with peak current output ≈35 μA in a single sliding to power the triboelectric immunotherapy. The pulsed direct-current stimulation induced immunogenic cell death of tumor cells (survival rate of 35.9 %), which promoted dendritic cells maturation, accelerated the process of antigen presentation to CAR-T cells and enhanced the systemic adaptive immune response. Furthermore, triboelectric immunotherapy promoted M1-like macrophage polarization, reduced regulatory T cells differentiation and reprogrammed the tumor immunosuppressive microenvironment, which ultimately enhanced the efficacy of CAR-T cells to eradicate nearly 60 % of NALM6 solid tumor mass. Notably, considering that triboelectric immunotherapy is a safe and effective drug-free antitumor strategy, the combined therapy did not increase the burden of double-medication on patients.

1. Introduction

Chimeric antigen receptor (CAR) T cell therapy is a highly effective immunotherapy for hematological tumors by infusing genetically engineered modified T cells back into the patient's body to achieve targeted treatment of tumor [1–4]. Compared to hematological tumors, solid tumors cause approximately 90 % of cancer incidence. However, CAR-T cell therapy efficacy against most solid tumors remains challenge although the clinical trials have increased significantly in recent years. The tumor microenvironment (TME) is a major barrier to CAR-T cell therapy for solid tumors [5–10]. Specifically, the specific tumor microenvironment of solid tumors affects the migration, penetration and infiltration of CAR-T cells, so that keeping CAR-T cells in an immunosuppressive state and are unable to effectively exert anti-tumor effects [8,11,12]. Thus, tumor microenvironment regulation is an effective strategy to enhance the efficacy of CAR-T cell therapy against solid tumors.

Studies have shown that combining CAR-T cell therapy with some

* Corresponding author. Department of Orthopedics Trauma and Microsurgery, Zhongnan Hospital of Wuhan University, School of Pharmaceutical Sciences, Wuhan University, Wuhan 430071, China.
** Corresponding author. School of Chemistry and Materials Sciences & School of Pharmaceutical Sciences, South-Central Minzu University, Wuhan 430074, China.
*** Corresponding author.
E-mail address: jiangpeng@whu.edu.cn (P. Jiang).

https://doi.org/10.1016/j.biomaterials.2024.122871
Received 23 June 2024; Received in revised form 14 September 2024; Accepted 1 October 2024
Available online 2 October 2024

other therapies can synergistically enhance the anti-tumor efficacy of CAR-T cells against solid tumors by modulating the tumor microenvironment [13–15]. For example, Murty et al. found that local radiotherapy can improve vascular extravasation and tumor infiltration of CAR-T cells to enhance efficacy against glioblastoma [16]. Watanabe et al. combined a lysosomal adenovirus expressing tumor necrosis factor (TNF)-α and interleukin (IL)-2 with CAR-T to alter the immune status of host tumor by promoting M1 polarization of macrophages and dendritic cells (DCs) maturation to increase the infiltration of CAR-T cells into the tumor [17]. In addition, some chemotherapy can induce immunosuppressive cell clearance and alleviate immunosuppression, often as a pretreatment for clinical CAR-T cell therapy [18–20]. However, treatments such as radiotherapy carries a greater risk of radiation and damage to normal tissues, and chemotherapy has serious drug side effects.

Recently, our group developed a novel drug-free tumor electro-immunotherapy (defined as "Triboelectric Immunotherapy"), which directly damage tumor cells and recruit immune cells by applying pulsed direct-current generated by a small size fabric triboelectric nanogenerator (TENG). Triboelectric nanogenerator (TENG) is devices that convert biomechanical energy into electrical energy through the coupled effect of triboelectrification and electrostatic induction, and can be used as power sources for wearable and implantable biomedical devices. In recent years, TENGs have been applied to drug delivery, wound repair, and triboelectric immunotherapy et al. [21] The triboelectric immunotherapy does not require any drug injections and can induce immunogenic cell death (ICD) of tumor cells using pulsed direct current generated by the TENG, attract immune cells infiltration and reprogram immune microenvironment, ultimately achieving drug-free tumor ablation [21]. More importantly, drug-free triboelectric immunotherapy avoids the side effects that existed in traditional pharmacotherapy. Therefore, the combination of triboelectric immunotherapy and CAR-T cell therapy is expected to improve the efficacy of CAR-T cells against solid tumors through the reprogramming of immunosuppressive microenvironment caused by electrical stimulation, while avoiding the burden of double-medication on patients.

Herein, a synergistic combination therapy of CAR-T cell therapy and drug-free triboelectric immunotherapy against NALM6 solid tumor mass was proposed (Scheme 1). Anti-CD19 single-chain variable fragment (scfv) was chosen to be chimerically embedded on CAR-T cells for targeting the surface CD19 antigen of NALM6 cells, because CD19 is widely expressed on the surface of B-cell malignant tumor cells but not expressed in most normal tissues and blood cells. Clinical results showed that the complete response rate of CD19-targeting CAR-T to acute B-lymphoblastic leukemia was as high as 78 % [7,22]. A TENG (8 cm × 10 cm) that can generate a pulsed direct-current by coupling triboelectrification effect and electrostatic breakdown effect was fabricated to power the triboelectric immunotherapy. For the triboelectric immunotherapy, two electrical stimulation needles were inserted into the tumor site and connected to the positive and negative electrode of TENG, respectively. The pulsed direct current stimulation generated by the TENG can induce ICD in tumor cells, promote DCs maturation and present tumor-associated antigens to CAR-T cells to accelerate the induction of CAR-T cells differentiation into cytotoxic CD4/CD8 CAR-T cells. Notably, a triboelectric immunotherapy system not only induced the polarization of tumor-associated macrophages (TAMs) from M2-type to M1-type, but also reduced the differentiation of regulatory T (Treg) cells, reprogrammed the immunosuppressive tumor microenvironment, and increased the infiltration and accumulation of CAR-T cells into the tumor tissues, ultimately enhancing the efficacy of CAR-T cells to eradicate nearly 60 % of NALM6 solid tumor mass. Moreover, CAR-T cell also differentiated to memory T cells, which contribute to the formation

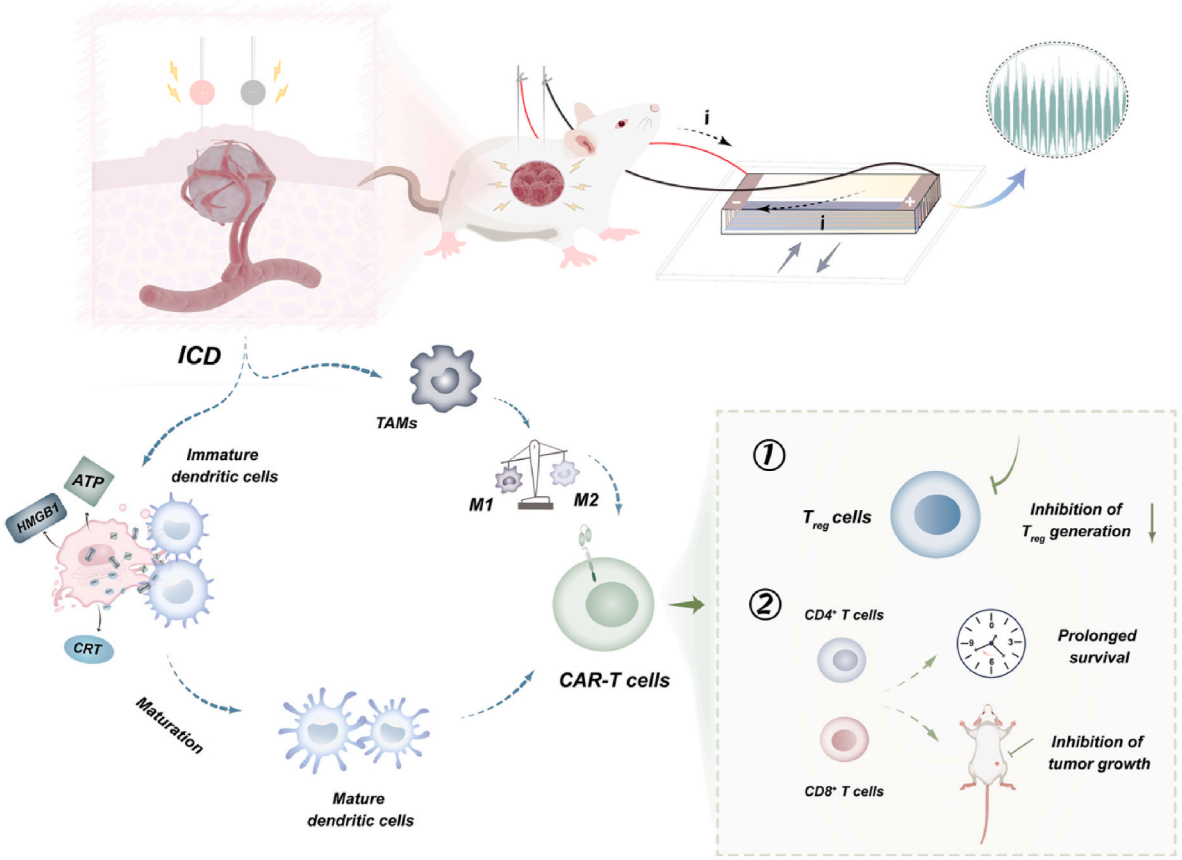

Scheme 1. Schematic illustration of CAR-T cell therapy against solid tumor enhanced by triboelectric immunotherapy-induced immunosuppressive microenvironment reprogramming.

of body's immune memory to prevent tumor metastasis and recurrence. The results demonstrated that the combined strategy can activate anti-tumor memory responses and avoid the burden of double-medication on patients.

2. Results and Discussion

Working mechanism and output performance of TENG. The schematic diagram and photograph of the TENG are shown in Fig. 1a and b. The TENG (8 × 10 cm) consists of 9 repeating units, each with a charge collecting electrode (CCE) and a frictional electrode (FE). In a typical device, a 2 mm wide copper foil was adhered to an acrylic substrate as a CCE layer, and a 3 mm wide copper foil was placed parallel to the CCE layer at a spacing of 1 mm as a FE layer, and a 0.3 mm thick polyurethane foam buffer layer (PORON 4701) was placed between the FE layer and acrylic substrate to create a vertical space between the CCE layer and the FE layer. When the direct-current (DC)-TENG slides on a polytetrafluoroethylene (PTFE) triboelectric layer, many pulsed direct-currents could be generated (Movie S1, Supporting Information).

Supplementary data related to this article can be found online at https://doi.org/10.1016/j.biomaterials.2024.122871

The working principle is similar to our previously reported work [21, 23]. Fig. 1c shows the schematic depiction of the TENG working principle. Initially, when the FE is in contact with the PTFE, the FE layer will be positively charged and the PTFE layer will be negatively charged due to the contact electrification (Fig. 1c, stage i), and the PTFE can hold the negative charge quasi-permanently. When sliding the DC-TENG on the PTFE film, partial positive charges will flow from FE to CCE, generating an extremely high electrostatic field between CCE and PTFE (Fig. 1c, stage ii). As long as the electrostatic field exceeds the dielectric strength of the air between them, electrons will flow from PTFE to CCE through the electrostatic breakdown process, generating pulsed direct-current output (Fig. 1c, stage iii). In this work, the TENG consisting of 9 repetitive units was used, and its open-circuit voltage (V_{OC}), short-circuit current (I_{SC}), and short-circuit charge transfer (Q_{SC}) can be achieved about 18 kV, 25 μA, and 1.28 μC per cycle, respectively (Fig. 1d–f). It is worth noting that the TENG can generate up to 30 pulse direct-current peaks in a single sliding (Fig. 1d), which are much more than the previous electrostatic-breakdown direct-current TENG and quite suitable for triboelectric immunotherapy [21].

ICD triggered by triboelectric immunotherapy *in vitro*. The killing effect of pulsed direct-current stimulation generated by TENG on tumor cells was verified by the MTT assay. The *in vitro* experimental setup was similar to previous report [21]. Firstly, tumor cells suspension was collected and placed in an electroporation cup connected with the two electrodes of the TENG. The pulsed current is applied to the electroporation cup during the treatment. Subsequently, cell viability of NALM6 cells treated with different electrical stimulation time was measured after 48 h static incubation (Fig. 2a). The results showed that the survival rate of NALM6 cells continued to decrease as a function of electrical stimulation time. The survival rate of cells was decreased to 28.7 % after 10 min electrical stimulation. Extending the stimulation time to 20 min further enhanced the effect, but the increase was not significant. It is worth noting that prolonged electrical stimulation may have side effects on normal tissues and reduce compliance. Taking this into consideration, we chose 10 min as the optimal stimulation time. Then, the effect of sliding frequencies on viability of NALM6 cells was evaluated with an electrical stimulation time of 10 min. As shown in Fig. 2b, NALM6 cell survival rate decreases progressively with increasing sliding frequency. In addition, tumor cell survival gradually decreased with incubation time, demonstrating that electrical stimulation-induced cell death did not occur instantaneously (Fig. S1). Notably, electrical stimulation also had a significant killing effect on other tumor cells (MOLM13 cells, HeLa cells and 4T1 cells), while causing slight damage to normal cells (293 cells, COS7 cells, RAW264.7 cells, HUVEC cells) (Fig. S2), which demonstrates the minimal side effects of our proposed therapy.

It has been extensively documented that pulsed electrical stimulation

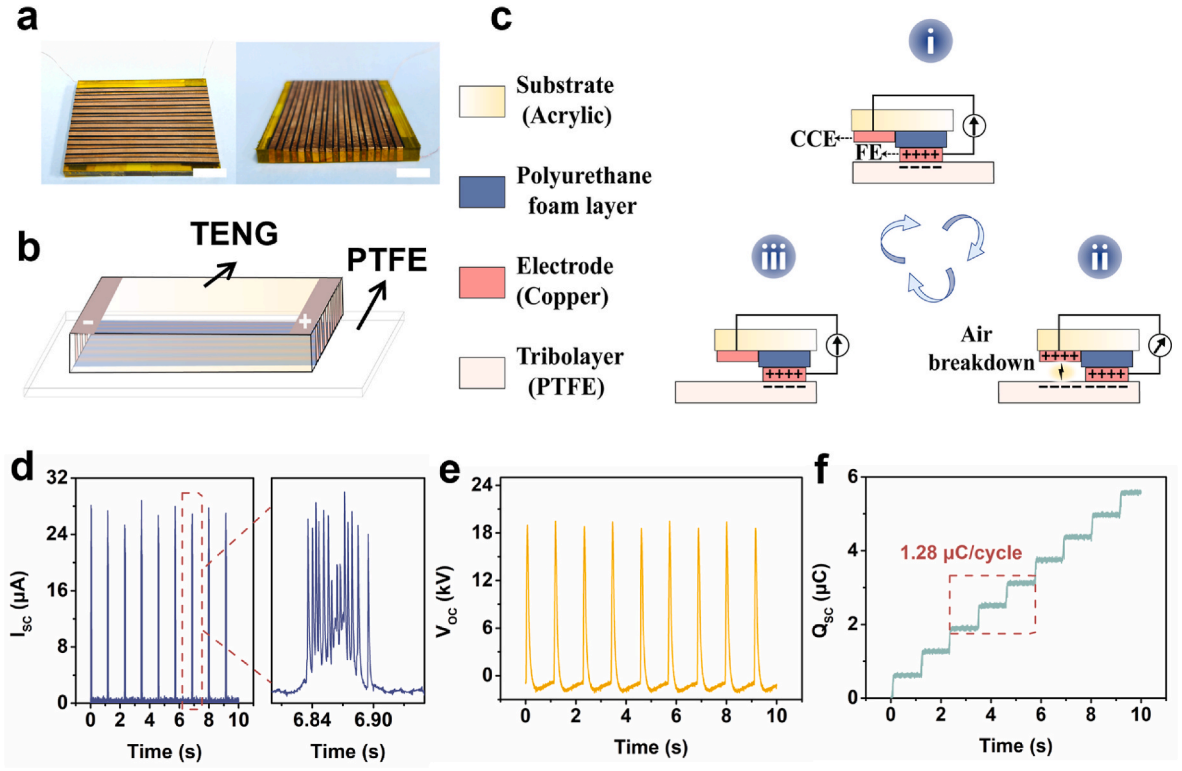

Fig. 1. Working mechanism and output performance of TENG. a) Photograph and b) schematic diagram of TENG. Scale bar: 2 cm. c) schematic illustration of the working mechanism, d) short-circuit current (I_{SC}), e) open-circuit voltage (V_{OC}) and f) short-circuit charge transfer (Q_{SC}) of TENG.

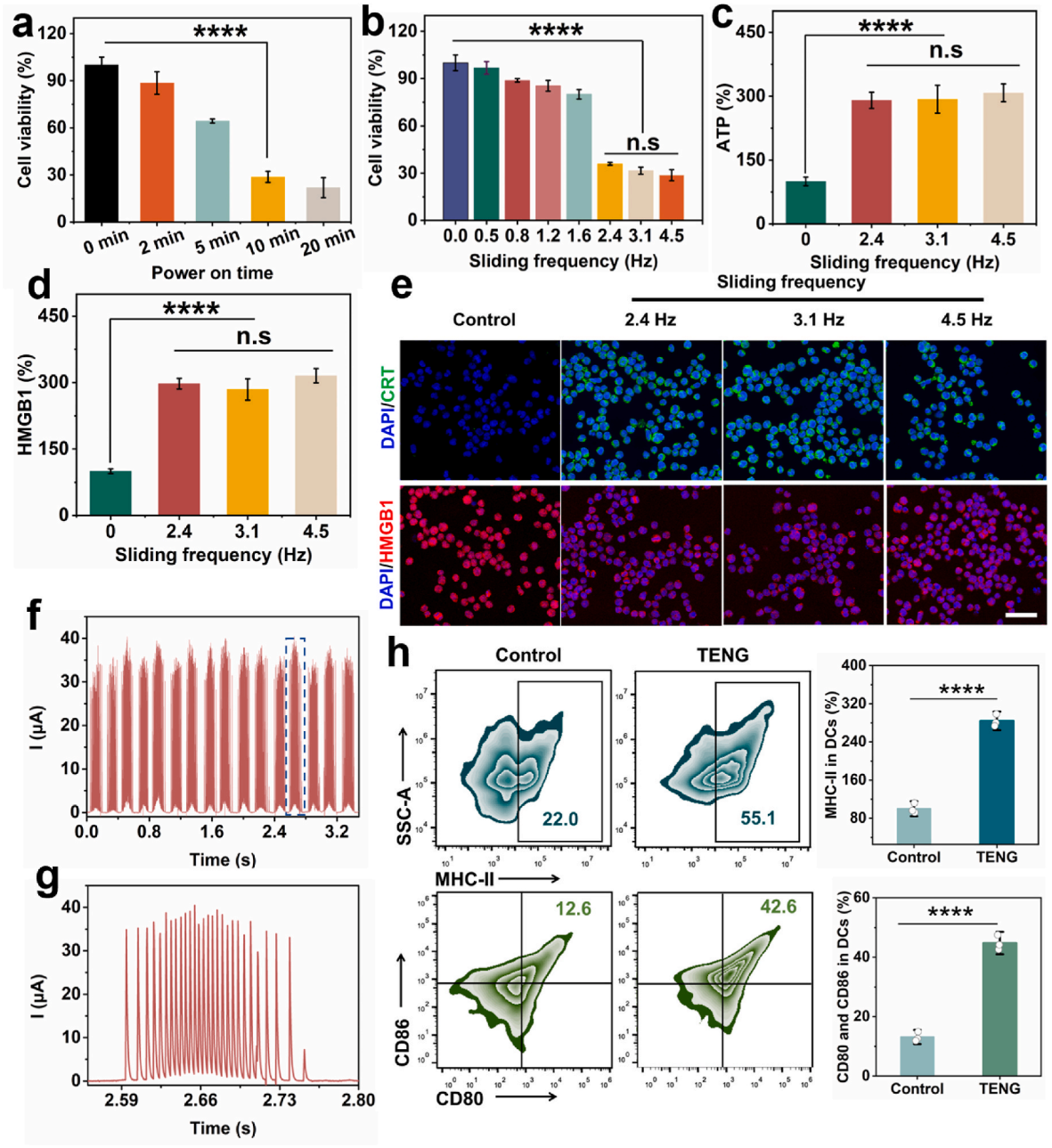

Fig. 2. Pulsed electrical stimulation-induced ICD and DCs maturation *in vitro*. a) Cell viability of NALM6 cells treated with electrical stimulation for 0 min, 2 min, 5 min, 10 min, 20 min at sliding frequency of 4.5 Hz. b) Cell viability of NALM6 cells treated with electrical stimulation generated by different sliding frequencies for 10 min. Relative percentage of c) ATP and d) HMGB1 content released to the extracellular environment of NALM6 cells with different treatments. e) Representative fluorescence microscopy images of CRT (green fluorescence) and HMGB1 (red fluorescence) expressed by NALM6 cells under electrical stimulation. Scale bar: 50 μm. f) Current output during *in vitro* electrical stimulation treatment, and (g) enlarged image of a single cycle current. h) Representative FACS of CD80/CD86, MHC-II expressed on the surface of mature DCs and corresponding quantitative analysis. *n.s.* not significant, $^{*}p < 0.1$, $^{**}p < 0.01$, $^{***}p < 0.001$, $^{****}p < 0.0001$. (For interpretation of the references to colour in this figure legend, the reader is referred to the Web version of this article.)

can cause ICD in tumor cells to induce the release of abundant tumor-associated antigens and damage-associated molecular patterns (DAMPs), such as exposure of calreticulin (CRT) to the cell surface, release of ATP and high-mobility group box 1 (HMGB1) to the external environment [24–26]. As shown in Fig. 2cd, the ATP and HMGB1 contents in the medium in the electrical stimulation treated group with sliding frequency of 2.4 Hz were 2.9- and 3.0-fold of the control group, respectively, indicating that electrical stimulation induced the release of large amounts of ATP and HMGB1 from the tumor cells into the external environment. Additionally, fluorescence microscopy imaging results showed that electrical stimulation induced strong green fluorescence of CRT and strong red fluorescence of HMGB1 from nucleus to extracellular (Fig. 2e).

Interestingly, there was no significant difference in ATP, HMGB1 and CRT content among the three electrical stimulation treated groups with sliding frequencies of 2.4 Hz, 3.1 Hz, and 4.5 Hz, suggesting that the low sliding frequency of 2.4 Hz is sufficient to induce significant ICD in tumor cells and achieve excellent tumor killing effect. Such a low sliding frequency can be achieved by manual sliding, and the current output by manual sliding have more pulsed current in single sliding with peak current output ≈35 μA (Fig. 2fg). Therefore, in the following experiment, the TENG was operated by manual sliding.

Notably, highly expressed signaling molecules (ATP, CRT, HMGB1) act as important signals for attracting DCs to recruitment and maturation, which can promote the phagocytosis of dead cancer cells and debris by DCs [21,27]. Thus, flow cytometry analysis (FACS) was used to evaluate the immunological effects of electrical stimulation on promoting DCs maturation and antigen presentation (Fig. 2h). The results demonstrated that the pulsed direct-current generated by TENG triggered a higher level of DCs maturation, which amplified the expression of major histocompatibility complex (MHC)-II on the surface of DCs and facilitated the recognition of DCs-presented antigens by CAR-T cells thus generating the first signal of T cell activation (Fig. 2h, top) [28]. Furthermore, the co-stimulatory molecules CD80 and CD86 expressed on the surface of the DCs, which were the second signals that activated the T cells, were also measured (Fig. 2h, bottom). The results showed that the expression of CD80 and CD86 were significantly amplified under electrical stimulation compared to control group. Both of these signals can synergistically elicit the activation of T cells and initiate adaptive immunity [29,30].

Immunological effects of triboelectric immunotherapy-induced macrophage polarization *in vitro*. Differentiation of immune cells and secreted cytokines construct the ramparts of host defense. Pulsed electrical stimulation treated tumor cells come to the edge of ICD, and the release of large-scale DAMPs can induce immune activation, induce conversion of M2-like macrophages to M1-type, and alter the expression of relevant proteins and cytokine secretion on the cell surface (Fig. 3ab) [31–33]. The macrophage polarization in triboelectric immunotherapy was studied in a Transwell system, where NALM6 cells were inoculated in the upper chamber with electrical stimulation treatment and

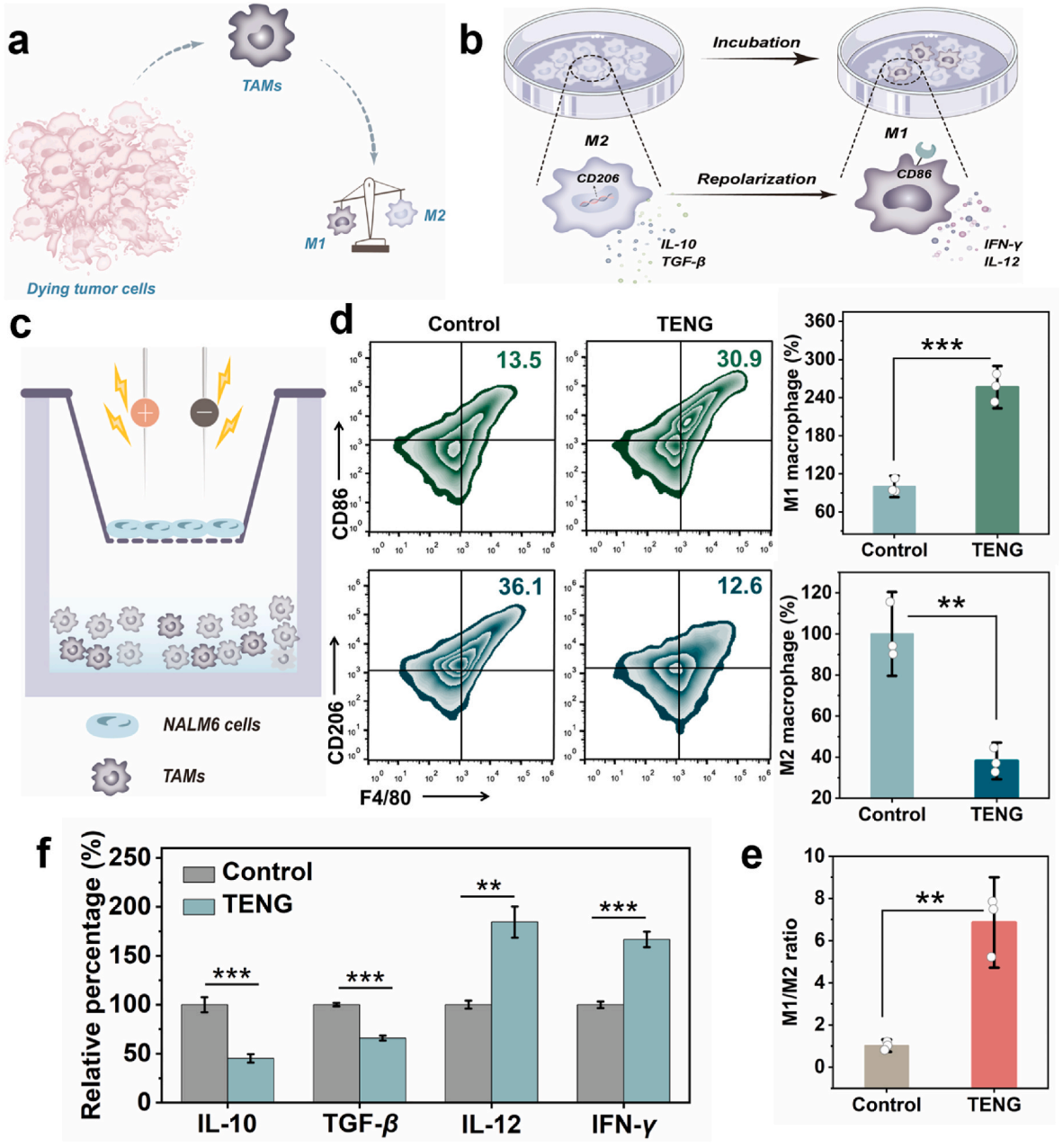

Fig. 3. Pulsed electrical stimulation-induced macrophage polarization *in vitro*. Schematic representation of (a) macrophage polarization mediated by electrical stimulation, and (b) the expression of relevant proteins and cytokine secretion in polarized macrophages. (c) Design of the Transwell system for studying macrophage polarization. (d) Representative FACS of macrophage differentiation into M1 and M2 macrophages, and (e) the corresponding M1/M2 ratio. (f) Relative percentages of cytokines secreted by polarized macrophages. *n.s.* not significant, $*p < 0.1$, $**p < 0.01$, $***p < 0.001$, $****p < 0.0001$.

RAW264.7 macrophages were co-incubated in the lower chamber (Fig. 3c). After incubated for 48 h, FACS was used to determine surface markers of RAW264.7 cells [34]. As shown in Fig. 3d, the positive rate of the M1 phenotype (F4/CD80$^+$CD86$^+$) significantly increased after electrical stimulation treatment (TENG group), whereas the positive rate of the M2 phenotype (F4/CD80$^+$CD206$^+$) significantly decreased. TENG treated group caused a 6.8-fold increase in the M1/M2 ratio relative to the Control group (Fig. 3e), indicating that TENG-mediated pulsed electrical stimulation caused effective polarization on TAMs. In addition, TENG treatment increased secretion of interferon (IFN)-γ and IL-12 (the main cytokines secreted by M1-like macrophages) and decreased production of transforming growth factor (TGF)-β and IL-10 (the main cytokine secreted by M2-like macrophages) (Fig. 3f) [35]. All these results demonstrated that TENG-mediated pulsed electrical stimulation can trigger ICD to promote macrophage polarization to M1 phenotype, which contribute to activation of the body's immune response [28].

Combination therapy-mediated CAR-T cells activation and differentiation *in vitro*. Differentiation of CAR-T cells is crucial in activating the body's anti-tumor immune response. Immunomodulatory CD4$^+$ CAR-T cells and cytotoxic CD8$^+$ CAR-T cells, as two characteristic manifestations of CAR-T cells activation and differentiation, are the main effectors trigger the systemic anti-tumor immune response [36,37]. Therefore, FACS was used to evaluate the effect of triboelectric immunotherapy on CAR-T cells differentiation. As shown in Fig. 4a, the number of CD4/CD8 CAR-T cells were 2.5- and 2.8-folds higher than that of Control group, respectively, indicating that triboelectric immunotherapy treatment promoted the CAR-T cells differentiation. Importantly, the activated CAR-T cells induced a massive burst of granzyme B, perforin, TNF-α and IFN-γ (Fig. 4b), which can mediate potent tumor cell killing and accelerate the process of tumor cell death [28,38]. In addition, highest single agent (HSA) and Bliss additive models were used to identify the combined antiproliferative effect between triboelectric immunotherapy and CAR-T cell therapy. As expected, the HSA and Bliss algorithms showed positive synergistic scores (Fig. 4c–e), identifying a synergistically enhanced anti-tumor effect between triboelectric immunotherapy and CAR-T cell therapy [39]. This exciting result motivates us to explore the anti-tumor therapeutic capabilities under combined therapy *in vivo*.

Combined therapy for NALM6 tumor mass *in vivo*. The anti-tumor performance of the combined triboelectric immunotherapy/CAR-T cell therapy for solid tumor was evaluated in NALM6 tumor mass bearing mice. As shown in Fig. S3, the finite element method was utilized to construct a tumor model with a diameter of 6 mm. The results showed that the ablation area of the simulated tumor increased with the increase of the distance between the two electrical stimulation needles. Even at distance of 5 mm between the two needles, there is still an effective tumor ablation area, and this exciting result encourages us to apply the device to the treatment of solid tumors. Firstly, NALM6 tumor-bearing mice were constructed and randomly divided into four groups (Fig. 5a), where Control group were injected intravenously with PBS (100 μL). In TENG group and TENG + CAR-T group, pulsed electrical stimulation generated from TENG was applied to tumors for 10 min every four days (Fig. S4, Movie S2), and the current output remains stable after 14 days (Fig. S5). The CAR-T cells (density 1.5 × 10^6)

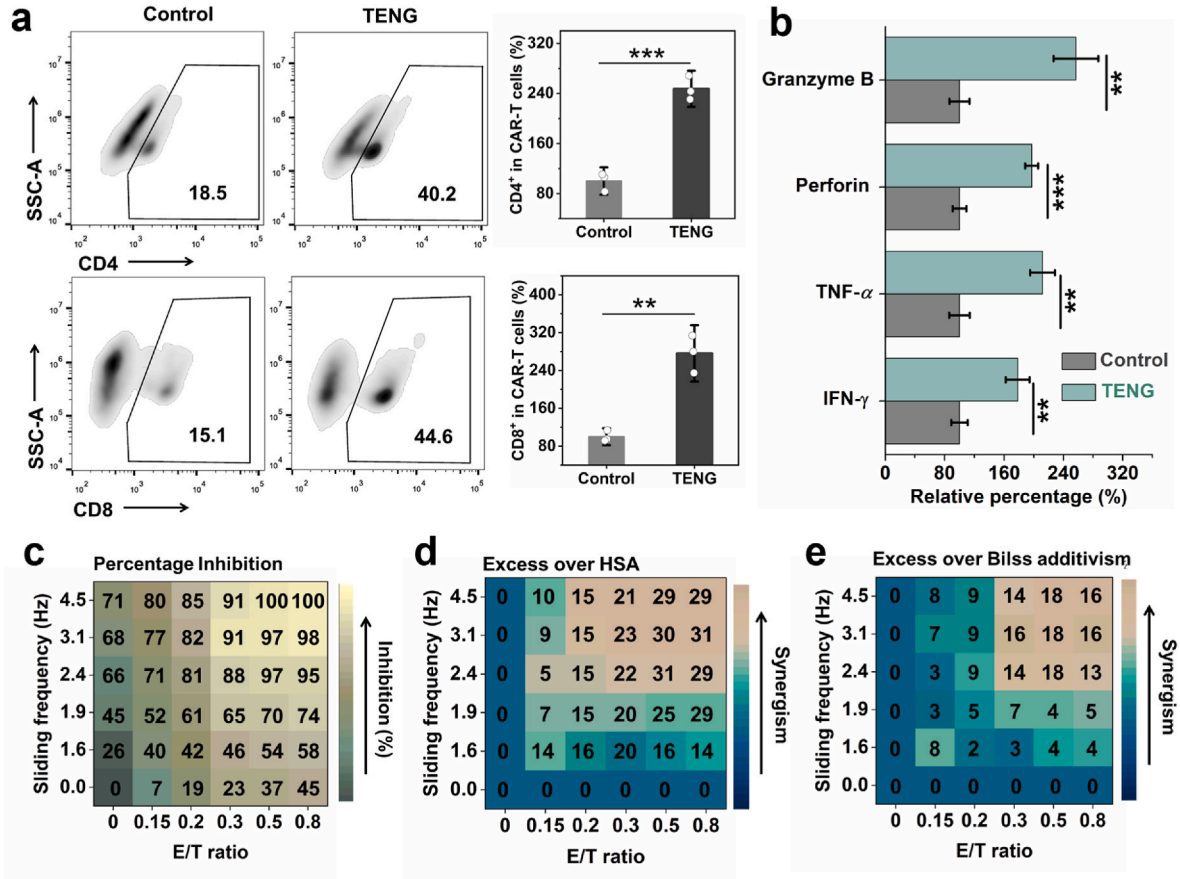

Fig. 4. Differentiation of CAR-T cells enhanced by triboelectric immunotherapy and their synergistic effect *in vitro*. (a) FACS and corresponding quantitative analysis of CD4/CD8 T cell on CAR-T cell differentiation with or without TENG treatment. (b) Percentage of granzyme B, perforin, TNF-α and IFN-γ after co-incubation of tumor cells with CAR-T cells. (c) Percent inhibition of CAR-T-mediated NALM6 cells with different effector-target ratios (E:T) at different sliding frequencies. (d) Differences in percentage inhibition of NALM6 cells under triboelectric immunotherapy or CAR-T cell therapy. (e) The differences between the actual value of measurement and each value predicted by Bliss additive model. *n.s.* not significant, *$p < 0.1$, **$p < 0.01$, ***$p < 0.001$, ****$p < 0.0001$.

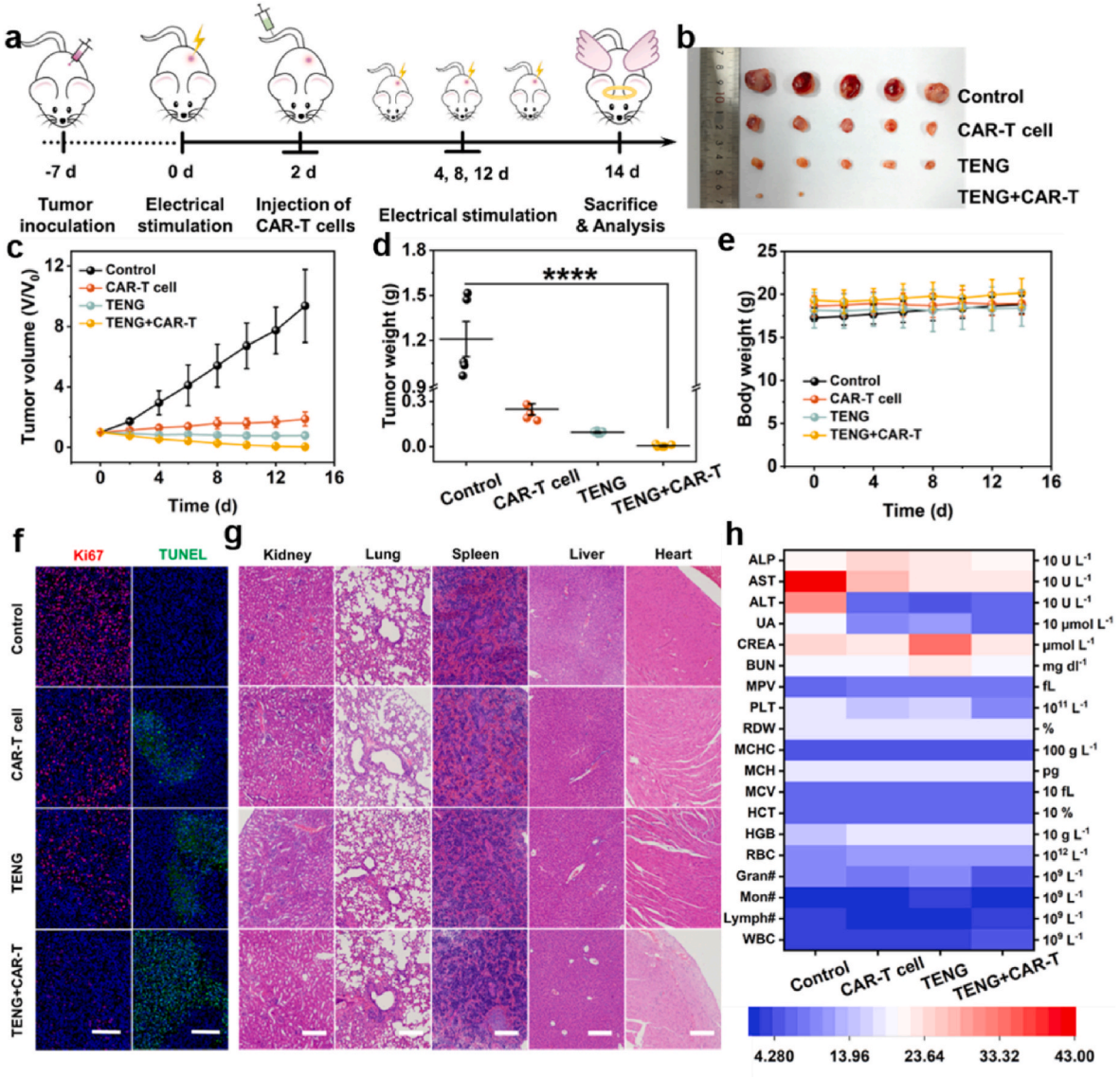

Fig. 5. Triboelectric immunotherapy synergistically enhanced CAR-T cell therapy against solid tumor *in vivo*. (a) Schematic diagram of the experimental design of the combined treatment with triboelectric immunotherapy and CAR-T cell therapy. (b) Photographs, (c) tumor volumes, (d) tumor weight of tumors from individual mice after 14 days of treatment in Control, CAR-T cell, TENG, TENG + CAR-T group. (e) Body weight of mice in different groups during treatment. (f) Representative Ki67 and TUNEL staining fluorescent images of tumor tissues, (g) representative images of H&E staining in mice main organs (kidney, lung, spleen, liver, heart), and (h) Heatmap of hematological analysis of mice from different groups. Scale bar: 100 μm. *n.s.* not significant, $^{*}p < 0.1$, $^{**}p < 0.01$, $^{***}p < 0.001$, $^{****}p < 0.0001$.

infusion in the CAR-T group and the TENG + CAR-T group was performed on the second day of the first electrical stimulation, and the signs data of mice were observed and recorded each two days [28]. After 14 days treatment, all mice were sacrificed and the relevant data were recorded (Fig. 5). As shown in Fig. 5b–d, rapid tumor growth was observed in the control group. Although the tumor growth in the CAR-T group was significantly suppressed, the tumor still grew persistently because the anti-tumor ability of CAR-T cells was suppressed by the harsh tumor microenvironment [40]. Surprisingly, the combination of triboelectric immunotherapy with CAR-T cell therapy in TENG + CAR-T group demonstrated a desirable enhancement in anti-tumor effect, resulting in eradication of 60 % of NALM6 solid tumor mass. The tumor-killing effect of the combined therapy were further verified by Ki67 and TUNEL staining [41]. As shown in Fig. 5f, Ki67 staining of mice tumor tissues in TENG + CAR-T group showed weakest red fluorescence, indicating that the inhibition of tumor cell proliferation was the strongest under combined therapy. TUNEL staining also showed strongest green fluorescence, demonstrating that tumor cells had the highest apoptosis after combined therapy [42]. These data confirmed that triboelectric immunotherapy synergistically enhanced CAR-T cell therapy against solid tumor. In addition, no body weight loss is observed from the mice during a 14-day treatment window (Fig. 5e), and no significant lesions were observed in H&E staining of major organs in mice after end of treatment (Fig. 5g), indicating that the combined therapy had no serious systemic toxicity [15]. The blood and serum of mice were also collected for hematological analysis and biochemical indicator tests (Fig. 5h). The results showed that the number of white blood cells in the combined therapy treated mice was within the normal range, and there were no obvious abnormalities in liver and kidney function indexes, which further proved the good biological safety of the combined therapy [43].

Supplementary data related to this article can be found online at https://doi.org/10.1016/j.biomaterials.2024.122871

Anti-tumor immune response driven by CAR-T cell activation *in*

vivo. Triboelectric immunotherapy-induced tumor immunosuppressive microenvironment reprogramming can promote immune cell infiltration and differentiation [21]. As shown in Fig. 6a, immunofluorescence staining of treated mice tumor tissues demonstrated that electrical stimulation increased large-scale recruitment of CAR-T cells at the tumor site and further differentiation into cytotoxic $CD4^+/CD8^+$ CAR-T cells [15]. At the same time, activated CAR-T cells also kill cancer cells by secreting the cytokines TNF-α and IFN-γ (Fig. 6bc), activating the apoptosis signaling pathway and inducing the body's powerful CAR-T cell-mediated anti-tumor immune response [44]. Furthermore, CAR-T cells recruitment were further verified by FACS (Fig. 6d), which also demonstrated a 4.5-fold and 3.1-fold increase in the number of $CD4^+$ and $CD8^+$ CAR-T cell at the tumor site in the TENG + CAR-T group compared to the CAR-T group. In addition, Treg cells serve as one of the factors that maintain the tumor immunosuppressive microenvironment. FACS results proved that Treg cells numbers in the CAR-T + TENG group was significantly reduced than in the CAR-T group (Fig. 6e), indicating that triboelectric immunotherapy could improve immunosuppression in the tumor microenvironment and significantly improve the efficacy of CAR-T cell therapy in solid tumors [44,45]. Importantly, cytokine secretion and reprogramming of the immunosuppressive microenvironment also contribute to the differentiation of memory T cells. As shown in Fig. 6f, the levels of effector memory T cells (T_{EM}, $CD44^+CD62L^-$) and central memory T cells (T_{CM}, $CD44^+CD62L^+$) in the TENG + CAR-T group were significantly higher than in the CAR-T group, which demonstrated that the combined strategy of triboelectric immunotherapy and CAR-T cell therapy can activate more robust anti-tumor memory responses [46].

3. Conclusions

In summary, this work demonstrated that the TENG-mediated triboelectric immunotherapy designed significantly enhanced the efficacy of CAR-T cell therapy against solid tumors through reprogramming of the tumor microenvironment. The TENG can generate up to 30 pulse direct-current peaks with peak current output ≈35 μA in a single sliding to induce ICD of tumor cells (survival rate of 35.9 %), which not only facilitated the process of antigen presentation from mature DCs to CAR-T cells, but also induced the polarization of TAMs and the reduction of Treg cells differentiation, reprogrammed the immunosuppressive tumor microenvironment, and increased the infiltration and accumulation of CAR-T cells into the tumor tissues, ultimately enhancing the efficacy of CAR-T cells to eradicate nearly 60 % of NALM6 solid tumor mass. Moreover, the levels of effector memory T cells (T_{EM}, $CD44^+CD62L^-$) and central memory T cells (T_{CM}, $CD44^+CD62L^+$) was promoted by triboelectric immunotherapy, which demonstrated that the combined strategy can activate more robust anti-tumor memory responses. Furthermore, the biosafety assessments further confirmed that the combination therapy of CAR-T cell therapy and drug-free triboelectric immunotherapy is a safe and effective drug-free antitumor strategy. The present study provides a novel combination therapy strategy for CAR-T cell therapy against solid tumors and is expected to be developed into a wearable miniaturized therapeutic device.

4. Experimental section

Fabrication of the TENG. In a typical device, a 2 mm wide copper

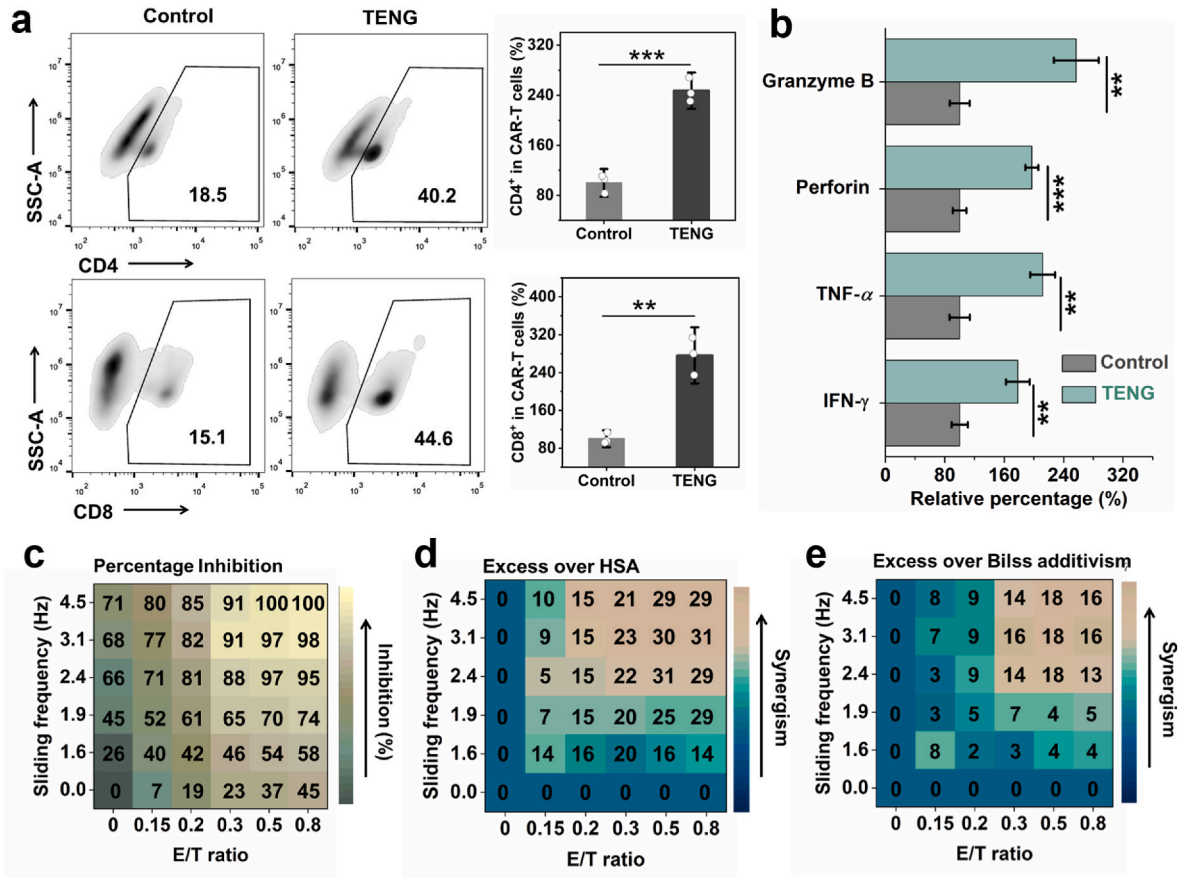

Fig. 6. Immune reprogramming-mediated immune activation of CAR-T cells *in vivo*. (a) Representative CD4 and CD8 immunofluorescence staining images of tumor tissues from different groups. Scale bar: 100 μm. Relative percentage of cytokines (b) TNF-α and (c) IFN-γ from tumor in different groups. Representative FACS of (d) $CD4^+/CD8^+$ T cell in tumor, and (e) Treg cell, (f) memory T cells in spleen, and corresponding quantitative analysis. *n.s.* not significant, $^*p < 0.1$, $^{**}p < 0.01$, $^{***}p < 0.001$, $^{****}p < 0.0001$.

foil (thickness: 60 μm) was adhered to an acrylic substrate as a CCE layer, and a 3 mm wide copper foil was placed parallel to the CCE layer at a spacing of 1 mm as a FE layer, and a 0.3 mm thick polyurethane foam buffer layer (PORON 4701) was placed between the FE layer and acrylic substrate to create a vertical space between the CCE layer and the FE layer.

Characterizations of the TENG. The open-circuit voltage, short-circuit current and short-circuit charge transfer at the output of the TENG during operation were characterized by a linear motor and an electrometer (Keithley 6514 system).

Cell culture section. NALM6 cells used in the experiments were from Gaining Biological Co. Ltd. (Shanghai, China), CAR-T cells were provided by Tongji Hospital of Huazhong University of Science and Technology. Specific cell culture protocols are listed in the Supporting I*nformation*.

Transwell System. The Transwell system was used to assess the differentiation of RAW264.7 macrophages and the maturation of DCs. Tumor cells inoculated in the upper chamber were treated with electrical stimulation (stimulation time: 10 min, sliding frequency: 2.4 Hz). Subsequently, macrophages or DCs in the lower chamber were co-incubated with the above treated tumor cells for 48 h. Finally, the cells were collected for analysis of cell surface protein expression by flow cytometry (FACS Calibur, BD), and the collected medium was measured with an ELISA detection kit (Jiangsu Meimian Industrial Co., Ltd) to measure the released cytokines (IL-10, TGF-β, IFN-γ, IL-12). Maker: anti-mouse CD80/FITC (1:200, bsm-30264A), anti-mouse CD86/PE (1:100, bsm-30264A), and anti-mouse MHC-II/FITC (1:200, bs-4107R), Anti-mouse CD206/PE (1:200, bsm-30276A-Percp-Cy5.5), Anti-mouse F4/CD80 (E-AB-F0995C, FITC).

Animal experimentation. Construction of tumor-bearing mice model. Humanized tumor-bearing mice carrying NALM6 solid tumor masses were constructed for subsequent *in vivo* experimental validation. Four experimental groups were set up: Control group, CAR-T group, TENG group and the TENG + CAR-T group ($n = 5$). Detailed construction protocols are listed in the Supporting *Information.*

Immunofluorescence staining analysis. After mice in all treatment groups were sacrificed, tumor tissues were collected for Ki67, TUNEL, $CD4^+$, and $CD8^+$ immunofluorescence staining. Maker: Anti-CD4 (1:200, ab183685), anti-CD8 (1:200, GB13429). Fluorescence microscopy (Nikon Eclipse C1, Japan) was used for imaging.

Flow analysis and ELISA analysis. Spleen and tumor tissues from four experimental groups of mice after euthanasia were collected for flow analysis and ELISA analysis, and the specific experimental protocols are listed in the *Supporting Information.*

CRediT authorship contribution statement

Haimei Li: Writing – original draft, Software, Funding acquisition, Formal analysis, Data curation. **Zichen Wang:** Software, Investigation, Data curation. **Yulin Hu:** Methodology, Data curation. **Guangqin He:** Validation, Software, Methodology, Data curation. **Liang Huang:** Validation, Data curation, Conceptualization. **Yi Liu:** Writing – review & editing, Validation, Software, Project administration, Funding acquisition. **Zhong Lin Wang:** Writing – review & editing, Project administration, Methodology, Data curation, Conceptualization. **Peng Jiang:** Writing – review & editing, Validation, Software, Methodology, Funding acquisition, Data curation, Conceptualization.

Declaration of competing interest

The authors declare that they have no known competing financial interests or personal relationships that could have appeared to influence the work reported in this paper.

Data availability

Data will be made available on request.

Acknowledgements

National Natural Science Foundation of China (U23A2089, 22403070, 22074113, 22073070), the Program of Science and Technology Plan of the City of Tianjin (No. 24JRRCRC00040), the China National Postdoctoral Program for Innovative Talents (BX20230268), the China Postdoctoral Science Foundation (2023M742690), the Young Top-notch Talent Cultivation Program of Hubei Province, and the Large-scale Instrument and Equipment Sharing Foundation of Wuhan University.

Appendix A. Supplementary data

Supplementary data to this article can be found online at https://doi.org/10.1016/j.biomaterials.2024.122871.

References

[1] M. Hong, J.D. Clubb, Y.Y. Chen, Engineering CAR-T cells for next-generation cancer therapy, Cancer Cell 38 (2020) 473–488, https://doi.org/10.1016/j.ccell.2020.07.005.
[2] P. Agarwalla, E.A. Ogunnaike, S. Ahn, K.A. Froehlich, A. Jansson, F.S. Ligler, G. Dotti, Y. Brudno, Bioinstructive implantable scaffolds for rapid *in vivo* manufacture and release of CAR-T cells, Nat. Biotechnol. 40 (2022) 1250–1258, https://doi.org/10.1038/s41587-022-01245-x.
[3] J.H. Park, I. Rivière, M. Gonen, X. Wang, B. Sénéchal, K.J. Curran, C. Sauter, Y. Wang, B. Santomasso, E. Mead, M. Roshal, P. Maslak, M. Davila, R.J. Brentjens, M. Sadelain, Long-term follow-up of CD19 CAR therapy in acute lymphoblastic leukemia, N. Engl. J. Med. 378 (2018) 449–459, https://doi.org/10.1056/NEJMoa1709919.
[4] V. Bhatia, N.V. Kamat, T.E. Pariva, L.-T. Wu, A. Tsao, K. Sasaki, H. Sun, G. Javier, S. Nutt, I. Coleman, L. Hitchcock, A. Zhang, D. Rudoy, R. Gulati, R.A. Patel, M. P. Roudier, L.D. True, S. Srivastava, C.M. Morrissey, M.C. Haffner, P.S. Nelson, S. J. Priceman, J. Ishihara, J.K. Lee, Targeting advanced prostate cancer with STEAP1 chimeric antigen receptor T cell and tumor-localized IL-12 immunotherapy, Nat. Commun. 14 (2023) 2041, https://doi.org/10.1038/s41467-023-37874-2.
[5] K. Adachi, Y. Kano, T. Nagai, N. Okuyama, Y. Sakoda, K. Tamada, IL-7 and CCL19 expression in CAR-T cells improves immune cell infiltration and CAR-T cell survival in the tumor, Nat. Biotechnol. 36 (2018) 346–351, https://doi.org/10.1038/nbt.4086.
[6] K.D. Kim, S. Bae, T. Capece, H. Nedelkovska, R.G. de Rubio, A.V. Smrcka, C.D. Jun, W. Jung, B. Park, T.I. Kim, M. Kim, Targeted calcium influx boosts cytotoxic T lymphocyte function in the tumour microenvironment, Nat. Commun. 8 (1) (2017) 15365, https://doi.org/10.1038/ncomms15365.
[7] S. Agarwal, M.A. Aznar, A.J. Rech, C.R. Good, S. Kuramitsu, T. Da, M. Gohil, L. Chen, S.-J.A. Hong, P. Ravikumar, A.K. Rennels, J. Salas-Mckee, W. Kong, M. Ruella, M.M. Davis, G. Plesa, J.A. Fraietta, D.L. Porter, R.M. Young, C.H. June, Deletion of the inhibitory co-receptor CTLA-4 enhances and invigorates chimeric antigen receptor T cells, Immunity 56 (2023) 2388–2407, https://doi.org/10.1016/j.immuni.2023.09.001.
[8] G.M. Delgoffe, C. Xu, C.L. Mackall, M.R. Green, S. Gottschalk, D.E. Speiser, D. Zehn, P.A. Beavis, The role of exhaustion in CAR T cell therapy, Cancer Cell 39 (2021) 885–888, https://doi.org/10.1016/j.ccell.2021.06.012.
[9] S.A. Rosenberg, N.P. Restifo, Adoptive cell transfer as personalized immunotherapy for human cancer, Science 348 (2015) 62–68, https://doi.org/10.1126/science.aaa4967.
[10] D. Romero, CAR T cells ready to go mainstream, Nat. Rev. Clin. Oncol. 13 (2016) 397, https://doi.org/10.1038/nrclinonc.2016.99, 397.
[11] J. Lemoine, M. Ruella, R. Houot, Born to survive: how cancer cells resist CAR T cell therapy, J. Hematol. Oncol. 14 (2021) 199, https://doi.org/10.1186/s13045-021-01209-9.
[12] R.C. Sterner, R.M. Sterner, CAR-T cell therapy: current limitations and potential strategies, Blood Cancer J. 11 (2021) 69, https://doi.org/10.1038/s41408-021-00459-7.
[13] A.J. Hou, L.C. Chen, Y.Y. Chen, Navigating CAR-T cells through the solid-tumour microenvironment, Nat. Rev. Drug Discov. 20 (2021) 531–550, https://doi.org/10.1038/s41573-021-00189-2.
[14] S. Rafiq, C.S. Hackett, R.J. Brentjens, Engineering strategies to overcome the current roadblocks in CAR T cell therapy, Nat. Rev. Clin. Oncol. 17 (2019) 147–167, https://doi.org/10.1038/s41571-019-0297-y.
[15] Y. Zhang, P. Pei, H. Zhou, Y. Xie, S. Yang, W. Shen, L. Hu, Y. Zhang, T. Liu, K. Yang, Nattokinase-mediated regulation of tumor physical microenvironment to enhance chemotherapy, radiotherapy, and CAR-T therapy of solid tumor, ACS Nano 17 (2023) 7475–7486, https://doi.org/10.1021/acsnano.2c12463.

[16] S. Murty, S.T. Haile, C. Beinat, A. Aalipour, I.S. Alam, T. Murty, T.M. Shaffer, C. B. Patel, E.E. Graves, C.L. Mackall, S.S. Gambhir, Intravital imaging reveals synergistic effect of CAR T-cells and radiation therapy in a preclinical immunocompetent glioblastoma model, OncoImmunology 9 (2020) e1757360, https://doi.org/10.1080/2162402x.2020.1757360.
[17] K. Watanabe, Y. Luo, T. Da, S. Guedan, M. Ruella, J. Scholler, B. Keith, R.M. Young, B. Engels, S. Sorsa, M. Siurala, R. Havunen, S. Tähtinen, A. Hemminki, C.H. June, Pancreatic cancer therapy with combined mesothelin-redirected chimeric antigen receptor T cells and cytokine-armed oncolytic adenoviruses, JCI Insight 3 (2018) e99573, https://doi.org/10.1172/jci.insight.99573.
[18] Y. Guo, K. Feng, Y. Liu, Z. Wu, H. Dai, Q. Yang, Y. Wang, H. Jia, W. Han, Phase I study of chimeric antigen receptor-modified T cells in patients with EGFR-positive advanced biliary tract cancers, Clin. Cancer Res. 24 (2018) 1277–1286, https://doi.org/10.1158/1078-0432.Ccr-17-0432.
[19] D.J. Baker, Z. Arany, J.A. Baur, J.A. Epstein, C.H. June, CAR T therapy beyond cancer: the evolution of a living drug, Nature 619 (2023) 707–715, https://doi.org/10.1038/s41586-023-06243-w.
[20] M.C. Milone, J. Xu, S.-J. Chen, M.A. Collins, J. Zhou, D.J. Powell, J.J. Melenhorst, Engineering-enhanced CAR T cells for improved cancer therapy, Nat. Cancer 2 (2021) 780–793, https://doi.org/10.1038/s43018-021-00241-5.
[21] H. Li, C. Chen, Z. Wang, Y. Huang, G. He, Y. Liu, P. Jiang, Z.L. Wang, Triboelectric immunotherapy using electrostatic-breakdown induced direct-current, Mater. Today 64 (2023) 40–51, https://doi.org/10.1016/j.mattod.2023.02.026.
[22] A.R. Saez-Ibañez, S. Upadhaya, T. Partridge, M. Shah, D. Correa, J. Campbell, Landscape of cancer cell therapies: trends and real-world data, Nat. Rev. Drug Discov. 21 (2022) 631–632, https://doi.org/10.1038/d41573-022-00095-1.
[23] D. Liu, X. Yin, H.Y. Guo, L.L. Zhou, X.Y. Li, C.L. Zhang, J. Wang, Z.L. Wang, A constant current triboelectric nanogenerator arising from electrostatic breakdown, Sci. Adv. 5 (2019) 8, https://doi.org/10.1126/sciadv.aav6437.
[24] E.J. Go, H. Yang, H.J. Chon, D. Yang, W. Ryu, D.H. Kim, D.K. Han, C. Kim, W. Park, Combination of irreversible electroporation and STING agonist for effective cancer immunotherapy, Cancers 12 (2020) 3123, https://doi.org/10.3390/cancers12113123.
[25] N. Zhang, Z. Li, X. Han, Z. Zhu, Z. Li, Y. Zhao, Z. Liu, Y. Lv, Irreversible electroporation: an emerging immunomodulatory therapy on solid tumors, Front. Immunol. 12 (2022) 811726, https://doi.org/10.3389/fimmu.2021.811726.
[26] C. He, X. Huang, Y. Zhang, X. Lin, S. Li, T-cell activation and immune memory enhancement induced by irreversible electroporation in pancreatic cancer, Clin. Transl. Med. 10 (2020) e39, https://doi.org/10.1002/ctm2.39.
[27] J. Zhao, X. Wen, L. Tian, T. Li, C. Xu, X. Wen, M.P. Melancon, S. Gupta, B. Shen, W. Peng, C. Li, Irreversible electroporation reverses resistance to immune checkpoint blockade in pancreatic cancer, Nat. Commun. 10 (2019) 899, https://doi.org/10.1038/s41467-019-08782-1.
[28] H. Li, X. Yang, Z. Wang, W. She, Y. Liu, L. Huang, P. Jiang, A near-infrared-II fluorescent nanocatalyst for enhanced CAR T cell therapy against solid tumor by immune reprogramming, ACS Nano 17 (2023) 11749–11763, https://doi.org/10.1021/acsnano.3c02592.
[29] B. Geboers, H.J. Scheffer, P.M. Graybill, A.H. Ruarus, S. Nieuwenhuizen, R.S. Puijk, P.M. van den Tol, R.V. Davalos, B. Rubinsky, T.D. de Gruijl, D. Miklavčič, M. R. Meijerink, High-voltage electrical pulses in oncology: irreversible electroporation, electrochemotherapy, gene electrotransfer, electrofusion, and electroimmunotherapy, Radiology 295 (2020) 254–272, https://doi.org/10.1148/radiol.2020192190.
[30] M. Lin, X. Zhang, S. Liang, H. Luo, M. Alnaggar, A. Liu, Z. Yin, J. Chen, L. Niu, Y. Jiang, Irreversible electroporation plus allogenic Vγ9Vδ2 T cells enhances antitumor effect for locally advanced pancreatic cancer patients, Signal Transduct. Tar. 5 (2020) 215, https://doi.org/10.1038/s41392-020-00260-1.
[31] M. Wang, M. Chang, P. Zheng, Q. Sun, G. Wang, J. Lin, C. Li, A noble AuPtAg-GOx nanozyme for synergistic tumor immunotherapy induced by starvation therapy-augmented mild photothermal therapy, Adv. Sci. 9 (2022) 2202332, https://doi.org/10.1002/advs.202202332.
[32] W. Chen, Y. Li, C. Liu, Y. Kang, D. Qin, S. Chen, J. Zhou, H.J. Liu, B.E. Ferdows, D. N. Patel, X. Huang, S. Koo, N. Kong, X. Ji, Y. Cao, W. Tao, T. Xie, In situ engineering of tumor-associated macrophages via a nanodrug-delivering-drug (β-Elemene@Stanene) strategy for enhanced cancer chemo-immunotherapy, Angew. Chem. Int. Edit. 62 (2023) e202308413, https://doi.org/10.1002/anie.202308413.
[33] X. Shi, B. Xiao, X. Xu, Y. Pan, J. Xiang, S. Shao, Z. Zhou, F. Huang, J. Gao, N.K. H. Slater, Y. Shen, J. Tang, Combination of cryo-shocked M1 macrophages and lonidamine nanodrugs enables potent chemo-immunotherapy, Adv. Funct. Mater. (2023) 2310364, https://doi.org/10.1002/adfm.202310364.
[34] L. Zhang, Y. Lin, S. Li, X. Guan, X. Jiang, In situ reprogramming of tumor-associated macrophages with internally and externally engineered exosomes, Angew. Chem. Int. Edit. 62 (2023) e202217089, https://doi.org/10.1002/anie.202217089.
[35] Y.D. Zhao, H.W. An, M. Mamuti, X.Z. Zeng, R. Zheng, J. Yang, W. Zhou, Y. Liang, G. Qin, D.Y. Hou, X. Liu, H. Wang, Y. Zhao, X. Fang, Reprogramming hypoxic tumor-associated macrophages by nanoglycoclusters for boosted cancer immunotherapy, Adv. Mater. 35 (2023) 2211332, https://doi.org/10.1002/adma.202211332.
[36] J. Qi, T. Ding, T. Liu, X. Xia, S. Wu, J. Liu, Q. Chen, D. Zhang, H. Zhao, Inosine-based supramolecular hydrogel for highly efficient PD-L1 blockade therapy via mediating $CD8^+$ T Cells, Adv. Funct. Mater. 32 (2022) 2204273, https://doi.org/10.1002/adfm.202204273.
[37] J. Huang, M. Wang, F. Zhang, S. Shao, Z. Yao, X. Zhao, Q. Hu, T. Liang, An ionic liquid ablation agent for local ablation and immune activation in pancreatic cancer, Adv. Sci. 10 (2023) 2206756, https://doi.org/10.1002/advs.202206756.
[38] Y. Qiu, Z. Wu, Y. Chen, J. Liao, Q. Zhang, Q. Wang, Y. Duan, K. Gong, S. Chen, L. Wang, P. Fan, Y. Duan, W. Wang, Y. Dong, Nano ultrasound contrast agent for synergistic chemo-photothermal therapy and enhanced immunotherapy against liver cancer and metastasis, Adv. Sci. 10 (2023) 2300878, https://doi.org/10.1002/advs.202300878.
[39] M. Dai, G. Yan, N. Wang, G. Daliah, A.M. Edick, S. Poulet, J. Boudreault, S. Ali, S. A. Burgos, J.J. Lebrun, *In vivo* genome-wide CRISPR screen reveals breast cancer vulnerabilities and synergistic mTOR/Hippo targeted combination therapy, Nat. Commun. 12 (2021) 3055, https://doi.org/10.1038/s41467-021-23316-4.
[40] L.H. Porter, J.J. Zhu, N.L. Lister, S.G. Harrison, S. Keerthikumar, D.L. Goode, R. Q. Urban, D.J. Byrne, A. Azad, I. Vela, M.S. Hofman, P.J. Neeson, P.K. Darcy, J. A. Trapani, R.A. Taylor, G.P. Risbridger, Low-dose carboplatin modifies the tumor microenvironment to augment CAR T cell efficacy in human prostate cancer models, Nat. Commun. 14 (2023) 5346, https://doi.org/10.1038/s41467-023-40852-3.
[41] H. Li, Y. Liu, B. Huang, C. Zhang, Z. Wang, W. She, Y. Liu, P. Jiang, Highly efficient GSH-responsive "Off-On" NIR-II fluorescent Fenton nanocatalyst for multimodal imaging-guided photothermal/chemodynamic synergistic cancer therapy, Anal. Chem. 94 (2022) 10470–10478, https://doi.org/10.1021/acs.analchem.2c01738.
[42] L. Zhu, J. Liu, G. Zhou, T.M. Liu, Y. Dai, G. Nie, Q. Zhao, Remodeling of tumor microenvironment by tumor-targeting nanozymes enhances immune activation of CAR T cells for combination therapy, Small 17 (2021) 2102624, https://doi.org/10.1002/smll.202102624.
[43] H. Li, M. Wang, B. Huang, S.-W. Zhu, J.-J. Zhou, D.-R. Chen, R. Cui, M. Zhang, Z.-J. Sun, Theranostic near-infrared-IIb emitting nanoprobes for promoting immunogenic radiotherapy and abscopal effects against cancer metastasis, Nat. Commun. 12 (2021) 7149, https://doi.org/10.1038/s41467-021-27485-0.
[44] W. Xie, B. Chen, H. Wen, P. Xiao, L. Wang, W. Liu, D. Wang, B.Z. Tang, Biomimetic nanoplatform loading type I aggregation-induced emission photosensitizer and glutamine blockade to regulate nutrient partitioning for enhancing antitumor immunotherapy, ACS Nano 16 (2022) 10742–10753, https://doi.org/10.1021/acsnano.2c02605.
[45] H. Chen, L. Liu, A. Ma, T. Yin, Z. Chen, R. Liang, Y. Qiu, M. Zheng, L. Cai, Noninvasively immunogenic sonodynamic therapy with manganese protoporphyrin liposomes against triple-negative breast cancer, Biomaterials 269 (2021) 120639, https://doi.org/10.1016/j.biomaterials.2020.120639.
[46] H. Zhao, L. Wang, K. Zeng, J. Li, W. Chen, Y.N. Liu, Nanomessenger-mediated signaling cascade for antitumor immunotherapy, ACS Nano 15 (2021) 13188–13199, https://doi.org/10.1021/acsnano.1c02765.